of ring strain energy that occurs as the first C–N bond of DBH is broken. As seen in Figure 5, this exothermicity lowers the energies of diazenyl states relative to DBH and makes the lowest excited diazenyl states energetically accessible. By contrast, acyclic azoalkanes prepared in their S_1 states cannot form electronically excited diazenyl radicals.[18] It seems likely that vapor-phase DBH shows an anomalously long S_1 lifetime and a structured absorption spectrum because its rigid covalent bridges prevent excited-state motion along the cis–trans twisting coordinate. In addition, this structural constraint would prevent DBH from photodissociating through twisted conformations, as we suspect occurs in acyclic azoalkanes.

The photodissociative quantum yield of DBH is much higher than that of the related compound 2,3-diazabicyclo[2.2.2]oct-2-ene (DBO), even though the two molecules differ by only one methylene group.[33] This surprising difference in behavior may be rationalized by using the same energetic and correlation considerations discussed above. Compared to DBH, the lower S_1–S_0 energy gap and higher thermolysis activation barrier of DBO combine to place its linear excited diazenyl biradical state approximately 5 kcal/mol higher than its S_1 origin energy. Thus, like DBH, optically excited DBO is inhibited from twisting about its double bond; but unlike DBH, it cannot reach the electronically excited diazenyl biradical and therefore has no adiabatic route for bond cleavage. With both of these decay channels obstructed, S_1 DBO shows an anomalously long lifetime and the highest fluorescence quantum yield known for any azoalkane.[33]

Conclusions

The photochemistry of DBH vapor excited to the origin of its S_1 state has been investigated by time-resolved spectroscopy on the nanosecond scale. Fluorescence lifetime measurements show the optically prepared state to undergo collision-free decay with a characteristic lifetime of slightly more than 2 ns. Time-resolved CARS measurements reveal that molecular nitrogen is produced from a precursor whose lifetime is approximately 25 ns. The unrelaxed nitrogen photoproduct molecules, when compared to those formed from azomethane, show a very similar vibrational state distribution but a significantly cooler rotational distribution. CARS spectroscopy has been used to monitor appearance kinetics of the bicyclopentane photoproduct, revealing a precursor lifetime of 195 ns. We interpret this value as the first-order lifetime of the triplet 1,3-cyclopentanediyl biradical against decay through ring closure.

The photochemical mechanism proposed to account for these findings involves stepwise breaking of the two C–N bonds. We view the first step as adiabatic formation of an excited singlet state of the diazenyl biradical from optically prepared S_1 DBH. The excited diazenyl singlet is then thought to undergo rapid intersystem crossing to the corresponding excited diazenyl triplet, which lives for 25 ns before predissociating into N_2 plus the lowest triplet state of the 1,3-cyclopentanediyl biradical. We interpret the cool rotational distribution of the N_2 photoproduct as reflecting the linear C–N–N structure that is characteristic of the predissociating diazenyl excited state.

These findings and the proposed mechanism apply to vapor-phase photodissociation of S_1 DBH in the presence of low to moderate buffer gas pressures, but not necessarily to solution photolysis, where a singlet channel seems to dominate. Further time-resolved experiments capable of intercepting diazenyl intermediates will be needed to understand this difference and to confirm the proposed gas-phase mechanism.

Acknowledgment. We are grateful to the National Science Foundation and the Robert A. Welch Foundation for research support. Our time-resolved fluorescence data were obtained at the Center for Fast Kinetics Research, which is supported jointly by the Biomedical Research Technology Program of the Division of Research Resources of NIH (RR00886) and by the University of Texas at Austin. We are also pleased to thank B. K. Andrews and K. A. Burton for valuable discussions and for their computational and experimental contributions.

Structures of X_2F_4, from Carbon to Lead. Unsaturation through Fluorine Bridges in Group 14

Georges Trinquier* and Jean-Claude Barthelat

Contribution from the Laboratoire de Physique Quantique, C.N.R.S., U.R.A. No. 505, Université Paul-Sabatier, 31062 Toulouse Cedex, France. *Received January 5, 1990*

Abstract: The various isomers of X_2F_4 with X = C, Si, Ge, Sn, and Pb are investigated through ab initio calculations using effective core potentials and taking into account part of the relativistic effects for tin and lead atoms. Geometries are determined at the SCF level and their relative energies are refined through CI calculations. The planar π-bonded structure $F_2X{=}XF_2$ is found to be a true minimum on the C_2F_4 potential energy surface, a saddle point on the Si_2F_4, Ge_2F_4, and Sn_2F_4 surfaces, and a true minimum on the first singlet excited Pb_2F_4 surface. The F_3X–XF isomer is found to be a true minimum in all cases but lead. Two nearly degenerate doubly bridged structures, cis and trans, are found to be true minima in all cases but carbon. The preferred isomers are tetrafluoroethylene for C_2F_4, tetrafluorosilylsilylene for Si_2F_4, and the trans-bridged structures for Ge_2F_4, Sn_2F_4, and Pb_2F_4. The diradical triplet species $F_2\dot{X}$–$\dot{X}F_2$ are always found to be significantly higher in energy than the preferred singlet ground-state forms. With respect to two singlet XF_2 fragments, the bridged structures have binding energies that increase regularly along the series from 3 kcal/mol in Si_2F_4 to 62 kcal/mol in Pb_2F_4, whereas bridged C_2F_4 is largely unbound. The potential wells corresponding to the bridged structures are found to be rather flat, possibly inducing small distortions associated to very slight energy changes. The in-plane $C_{2h} \rightarrow C_i$ deformation found for the planar four-membered ring of Ge_2F_4 is in agreement with its solid-state geometry. A structural and energetic comparison is made within group 14 between the fluorine bridges in X_2F_4 and the hydrogen bridges in X_2H_4. Some results are compared with spectroscopic data available for the monomers and dimers of SnF_2 and PbF_2.

I. Introduction

While tetrafluoroethylene has been the target of many theoretical studies related to its structure[1,2] or its weak C=C bond energy,[3-5] there is much less structural and theoretical work on its heavier analogues in group 14. For Si_2F_4, a doubly bonded

(1) Dixon, D. A.; Fukunaga, T.; Smart, B. E. *J. Am. Chem. Soc.* **1986**, *108*, 1585.
(2) Heaton, M. M.; El-Talbi, M. R. *J. Chem. Phys.* **1986**, *85*, 7198.
(3) Carter, E. A.; Goddard, W. A., III, *J. Am. Chem. Soc.* **1988**, *110*, 4077.
(4) Schultz, P. A.; Messmer, R. P. *J. Am. Chem. Soc.* **1988**, *110*, 8258.
(5) Wang, S. Y.; Borden, W. T. *J. Am. Chem. Soc.* **1989**, *111*, 7282.

0002-7863/90/1512-9121$02.50/0

or diradical intermediate F_2SiSiF_2 has been proposed for the insertion reaction of SiF_2 into ethylenic or acetylenic bonds,[6] but no clear evidence for its existence was provided.[7] Krogh-Jespersen explored theoretically the Si_2F_4 potential energy surface at an ab initio level.[8] He found no closed-shell minimum corresponding to a Si=Si double link. The preferred arrangement was found to be the singlet silylsilylene form F_3Si–SiF, while a diradical triplet species $F_2\dot{S}i$–$\dot{S}iF_2$ was located 25 kcal/mol higher in energy. In that work, however, no bridged structure was explored, whereas such an arrangement is known to occur frequently in fluorine derivatives of heavier group 14 elements.[9-18] In keeping with the XF_2 stoichiometry, solid-state germanium difluoride GeF_2 consists of separate bridged dimers.[14-16] Such Ge_2F_4 molecular units have also been detected in the gas phase, where vibrational spectroscopy studies support a C_{2h} bridged structure like **1** for the dimer of GeF_2.[19] Such a form has also been put forward for the dimer

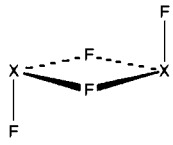

1

of SnF_2.[20,21] In the solid state, however, SnF_2 no longer forms dimer units like **1** but eight-membered-ring tetramers.[15,16] In contrast with these molecular arrangements, solid-state PbF_2 has a pure ionic crystal structure.[14,15] In the low-temperature modification (α-PbF_2), each Pb^{2+} ion is surrounded by nine F^- ions located at 2.41–3.03 Å. The high-temperature modification (β-PbF_2) has the fluorite structure, with each Pb^{2+} ion being surrounded by eight F^- located at 2.57 Å. While formation of bridged dimers has been proposed in gas-phase $PbCl_2$,[22,23] it seems that this does not occur with PbF_2, according to PES and mass spectroscopy studies.[20,24]

In previous modeling,[25] we showed that when the singlet–triplet separation ΔE_{ST} of an XR_2 fragment is larger than half the $\sigma + \pi$ X=X bond energy $E_{\sigma+\pi}$, i.e.

$$\Delta E_{ST} > \tfrac{1}{2}E_{\sigma+\pi} \qquad (1)$$

this is a presumption for nonexistence of XX bonded species such as $R_2X{=}XR_2$, a bridged structure being rather preferred for the dimer of XR_2. Such a naive model enabled us to predict the stability of the bridged structure of Pb_2H_4, in a preceding study of X_2H_4 molecules.[26] For group 14 difluorides, except for the case of carbon, ΔE_{ST} is larger than 70 kcal/mol whereas $E_{\sigma+\pi}$ is smaller than 80 kcal/mol ($E_{\sigma+\pi} \simeq$ 70–90 kcal/mol for Si=Si and expectedly lower for the heavier homopolar double bonds). Condition 1 is therefore largely satisfied, which provides an a priori rationale for the nonexistence of π-bonded species $F_2X{=}XF_2$ whenever silicon or heavier elements are involved.

Table I. Calculated Geometries and Relative Energies of the $^1A_1$ and $^3B_1$ States of XF_2[a]

		$^1A_1$		$^3B_1$		ΔE_{ST}	
		X–F	FXF	X–F	FXF	SCF	CI
CF_2	DZd	1.281	104.7	1.306	118.1	30.1	46.8
	DZdd	1.279	104.7	1.303	118.3	31.6	46.3
	exptl[b]	1.304	104.8				50 ± 2
SiF_2	DZd	1.611	99.1	1.610	113.5	55.6	71.1
	DZdd	1.598	99.5	1.596	114.0	55.3	71.0
	exptl[b]	1.590	100.8				75.2[d]
GeF_2	DZd	1.768	97.1	1.760	113.1	63.1	74.4
	DZdd	1.742	97.0	1.732	112.8	62.6	75.3
	exptl[b]	1.732	97.2				
SnF_2	DZd	1.913	96.0	1.903	112.5	64.4	73.6
	DZdd	1.889	95.7	1.878	111.8	63.8	73.7
PbF_2	DZd	2.109	98.7	2.100	122.9	80.9	86.1
	DZdd	2.091	98.2	2.060	118.9	83.1	88.4
	exptl[e]	2.033	97.8				

[a] Bond lengths in angstroms, bond angles in degrees, energies in kilocalories per mole. [b] Microwave spectroscopy.[34] [c] Lower bound;[35a] see also, refs 35b,c. [d] Reference 26. [e] Electron diffraction.[37]

In this paper, we present the results of a theoretical study of group 14 compounds XF_2 and their dimers X_2F_4 (X = C, Si, Ge, Sn, Pb). The geometries are determined at the SCF level by using pseudopotential techniques which include part of the relativistic effects for tin and lead atoms, since some of these effects are no longer negligible when $Z \geqslant 50$.[27,28] For the optimized geometries, energies are refined through configuration interaction (CI) calculations. For XF_2, we will stress the singlet–triplet splitting associated to the $^1A_1$ and $^3B_1$ low-lying states. For the dimers X_2F_4, we will consider four types of structures on the singlet surface, $F_2X{=}XF_2$, $FX{<}^{F}_{F}{>}XF$ (trans and cis isomers), and F_3X—XF, together with the diradical triplet species $F_2\dot{X}$—$\dot{X}F_2$. All along this work, a parallel will be made, as far as possible, between the X_2F_4 and the X_2H_4 potential energy surfaces.

II. Computational Details

Restricted Hartree–Fock (RHF) and spin-unrestricted Hartree–Fock (UHF) valence-shell calculations are carried out by using the PSHONDO algorithm,[29] which is derived from the standard HONDO program package[30] by introducing the pseudopotentials of Durand and Barthelat.[31] For tin and lead, we used effective core potentials taking into account mean relativistic effects through mass–velocity and Darwin term corrections.[31b]

Four atomic Gaussian functions are contracted in a double-ζ form for each atom.[32] Adding a d polarization function set to X defines the DZd basis set. The exponents for the d functions are taken at 0.80, 0.45, 0.25, 0.20, and 0.15 for C, Si, Ge, Sn, and Pb, respectively. A second basis set augmented with d polarization functions on F (η = 0.90) is also used to calculate the monomers.

Geometry optimizations are carried out at the SCF level by using a direct gradient technique. The convergence threshold for the gradient components was fixed at 10^{-4}. Unfortunately, optimized geometries for F_3X–XF ($^1A'$) and $F_2\dot{X}$–$\dot{X}F_2$ (^3B) could not reach this value and have some gradient components only lower than 10^{-3}. The triplet states of the

(6) Margrave, J. L.; Perry, D. L. *Inorg. Chem.* **1977**, *16*, 1820.
(7) Seyferth, D.; Duncan, D. P. *J. Am. Chem. Soc.* **1978**, *100*, 7734.
(8) Krogh-Jespersen, K. *J. Am. Chem. Soc.* **1985**, *107*, 537.
(9) Davies, A. G.; Smith, P. J. In *Comprehensive Organometallic Chemistry*; Wilkinson, G., et al., Eds.; Pergamon Press: Oxford, 1983; p 519.
(10) (a) Harrison, P. G. In *Comprehensive Organometallic Chemistry*; Wilkinson, G, et al., Eds.; Pergamon Press: Oxford, 1983; Vol. 2, p 629. (b) Harrison, P. G. In *Comprehensive Coordination Chemistry*; Wilkinson, G., et al., Eds.; Pergamon Press: Oxford, 1987; p 173.
(11) For a recent experimental structure of a Si–F–Si bridge, see: Tamao, K.; Hayashi, T.; Ito, Y. *J. Am. Chem. Soc.* **1990**, *112*, 2422.
(12) Mallouk, T. E.; Desbat, B.; Bartlett, N. *Inorg. Chem.* **1984**, *23*, 3160.
(13) Mallouk, T. E.; Rosenthal, G. L. Müller, G.; Brusasco, R.; Bartlett, N. *Inorg. Chem.* **1984**, *23*, 3167.
(14) Wells, A. F. *Structural Inorganic Chemistry*, 4th ed.; Clarendon Press: Oxford, 1975; pp 930, 222, 353.
(15) Greenwood, N. N.; Earnshow, A. *Chemistry of the Elements*; Pergamon Press: Oxford, 1984; p 438.
(16) Hargittai, M. *Coord. Chem. Rev.* **1988**, *91*, 35.
(17) For fluorine bridges on carbon atoms, see for instance: Hehre, W. J.; Radom, L.; Schleyer, P. v. R.; Pople, J. A. *Ab Initio Molecular Oribtal Theory*; John Wiley and Sons: New York, 1986.
(18) For fluorine bridges in transition-metal compounds, see: Massa, W.; Babel, D. *Chem. Rev.* **1988**, *88*, 275.
(19) Huber, H.; Kündig, E. P.; Ozin, G. A.; Vander Voet, A. *Can. J. Chem.* **1974**, *52*, 95.
(20) Zmbov, K.; Hastie, J. W.; Margrave, J. L. *Trans. Faraday Soc.* **1968**, *64*, 861.
(21) Hauge, R. H.; Hastie, J. W.; Margrave, J. L. *J. Mol. Spectrosc.* **1973**, *45*, 420.
(22) Schäfer, H.; Binnewies, M. *Z. Anorg. Allg. Chem.* **1974**, *410*, 251.
(23) Dewar, M. J. S.; Holloway, M. K.; Grady, G. L.; Stewart, J. P. *Organometallics* **1985**, *4*, 1973.
(24) Novak, I.; Potts, A. W. *J. Chem. Soc., Dalton Trans.* **1983**, 2211.
(25) Malrieu, J. P.; Trinquier, G. *J. Am. Chem. Soc.* **1989**, *111*, 5916.
(26) Trinquier, G. *J. Am. Chem. Soc.* **1990**, *112*, 2130.
(27) Pyykkö, P. *Chem. Rev.* **1988**, *88*, 563.
(28) Balasubramanian, K. *J. Phys. Chem.* **1989**, *93*, 6585.
(29) Pélissier, M.; Komiha, N.; Daudey, J. P. *J. Comput. Chem.* **1988**, *9*, 298.
(30) Dupuis, M.; King, H. F. *J. Chem. Phys.* **1978**, *68*, 3998.
(31) (a) Durand, Ph.; Barthelat, J. C. *Theor. Chim. Acta* **1975**, *38*, 283. (b) Barthelat, J. C.; Pélissier, M.; Durand, Ph. *Phys. Rev. A* **1981**, *21*, 1773.
(32) Molecular ab initio calculations using pseudopotentials. Technical Report, Laboratoire de Physique Quantique, Toulouse, 1981.

Table II. Calculated Harmonic Vibrational Frequencies (cm^{-1}) for $^1A_1$ Ground-State SnF_2 and PbF_2

	SnF_2		PbF_2	
	SCF	exptl[a]	SCF	exptl[a]
a_1 (sym stretch)	678	605	618	546
a_1 (bend)	221	201	162	170
b_2 (antisym stretch)	664	584	603	523

[a] Experimental values from Ne matrix measurements.[21]

XF_2 monomers and dimers are optimized by using the UHF version of the program. The value of $\langle S^2 \rangle$ always remains within 1% of $S(S+1)$, except for the Pb species [4% for PbF_2 ($^3B_1$) and 5% for F_2 $\dot{P}b$–$\dot{P}bF_2$ (^3B)]. For this reason PbF_2 ($^3B_1$) was treated by the open-shell RHF procedure. Harmonic vibrational frequencies are calculated from the analytical expression of the gradient, using a numerical evaluation of the second derivatives (single-point differencing formula).

Valence-shell configuration interaction calculations are performed for the SCF-optimized geometries with the CIPSI algorithm.[33] According to this procedure, a variational zeroth-order wavefunction is built-up from an iterative selection of the most important determinants. The remaining determinants are treated through a second-order Möller–Plesset perturbation. In the final step, we included in the zeroth-order wavefunction all determinants having a coefficient larger than 0.02 in the first-order wavefunction. If we consider the Ge-containing closed-shell species as a typical example, the subspaces that are variationally treated include ~25 determinants while the number of determinants involved in the perturbation treatment ranges from 4×10^6 to 9×10^6.

Supplementary calculations are carried out on the C_{2h} bridged structure of Ge_2F_4 in order to check the validity of our DZd description for the GeFGeF cycle. Adding a d polarization function to the bridging fluorine atoms induces geometry changes on the ring of only 1.8% for the bond distances and 2.5% for the angles. In the same way, the CI energy difference between this structure and two GeF_2 ($^1A_1$) monomers is reduced by no more than 3 kcal/mol.

III. Difluoride Monomers XF_2

The geometries and relative energies of the $^1A_1$ and $^3B_1$ states of XF_2 monomers are listed in Table I. On these systems, a basis set that includes a d function of the fluorine atoms has also been used (noted DZdd in Table I). Inclusion of d orbitals on fluorine affects the geometries and the singlet–triplet separations very little. The only significant effect is an expected shortening of the X–F distances by 0.02 Å (except for CF_2, where the effect is even smaller).

Along the series, there is a regular decrease in the F–X–F angles both on singlet and triplet species, except for PbF_2, the triplet state of which has a rather open angle (123°). A similar tendency had been observed[38] in the $^3B_1$ state of PbH_2 (θ = 119°) but it must be pointed out that the spin–orbit effects significantly reduce this value in the $^3B_1$ (A_1) spin–orbit state. Therefore, we must keep in mind that in $^3B_1$ PbF_2, the inclusion of spin–orbit coupling terms could similarly reduce our calculated valence angle. For singlet SnF_2 and PbF_2, the harmonic vibrational frequencies are given in Table II (DZd basis set) and compare well with those obtained in rare gas matrices.[21]

As expected, all the XF_2 species have a singlet ground state with increasing singlet–triplet splittings along the series. For CF_2, the calculated ΔE_{ST} is smaller than the experimental one, probably due to incomplete treatment of correlation.[39] For SiF_2, our calculated ΔE_{ST} is similar to that calculated by Krogh-Jespersen with analogous basis sets (71 kcal/mol).[8] Yet it is found 4 kcal/mol lower than the experimental value proposed by Rao.[36]

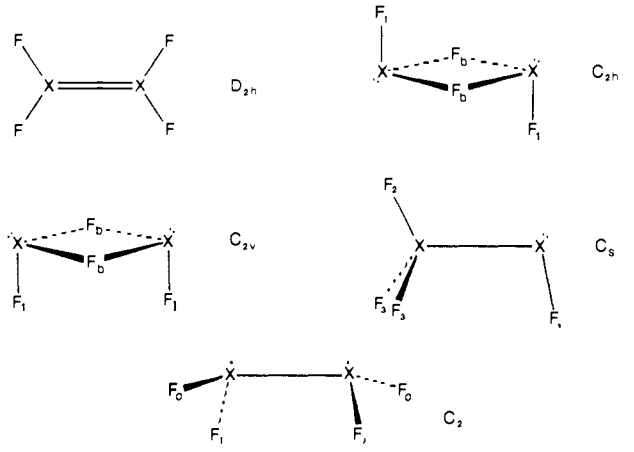

Figure 1. Definitions for the geometries.

The calculated ΔE_{ST} for GeF_2 is larger than that of SiF_2. Rather unexpectedly, the CI-calulated ΔE_{ST} for SnF_2 is smaller than that of GeF_2. This trend is observed with both basis sets. We checked whether this could come from an incomplete treatment of correlation. Performing refined CI calculations with a procedure that allows a variational treatment of very large configurational spaces[40] did not change the ΔE_{ST} in Table I for GeF_2 and SnF_2. Because relativisitc effects are included in the pseudopotential of tin and not in that of germanium, it cannot be settled if this unexpected ordering, with such a tiny difference (1 kcal/mol), is real or artifactual. Anyway what is sure is the very close values of ΔE_{ST} for GeF_2 and SnF_2. This is reminiscent of the close values of ΔE_{ST} calculated for GeH_2 and SnH_2, although the ΔE_{ST} gap was found to be larger for SnH_2.[26]

While SiF_2, GeF_2, and SnF_2 have quite close ΔE_{ST}, PbF_2 exhibits a larger ΔE_{ST} gap (86–88 kcal/mol). This is, to our knowledge, the largest singlet–triplet splitting ever found in such valence-isoelectronic XR_2 systems. The reason for the large ΔE_{ST} in PbR_2 systems comes from the inert-pair effect, which is a direct consequence of the relativistic contraction of the Pb 6s orbital.[27,28,38,41]

The first ionization potentials for the monomers SnF_2 and PbF_2 in their ground state were calculated by using Koopmans' theorem (KT) at 11.42 and 12.30 eV, respectively. Application of corrections for repolarization and corelation effects according to the procedure proposed in ref 42 leads to 11.66 eV for SnF_2 and 12.06 eV for PbF_2. These values confirm the assignments made on the PES spectra of SnF_2, but not those made on the PES spectra of PbF_2 (see below).[24]

IV. X_2F_4 Potential Energy Surfaces

A. Stationary Points. Five types of stationary points were explored on the X_2F_4 singlet potential energy surfaces: (1) the planar doubly bonded form, which is known to be the stable form for C_2F_4; (2) the trans-bent form, which is a real minimum on the parent disilene, digermene, and distannene surfaces; (3) the doubly bridged structures, trans (C_{2h}) **2** and cis (C_{2v}) **3**; and lastly

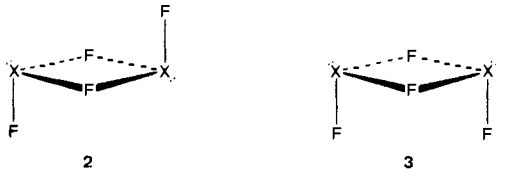

(4) the methylmethylene-type isomer, **4**. Besides this, a diradicalar twisted form of C_2 symmetry, **5**, has been explored on the triplet surface. Exploring the trans-bent region by imposing C_{2h} sym-

(33) Daudey, J. P.; Malrieu, J. P. In *Current Aspects of Quantum Chemistry*; Carbo, T., Ed.; Elsevier: Amsterdam, 1982; p 35.
(34) Harmony, M. D.; Laurie, V. W.; Kuczkowski, R. L.; Schwendeman, R. H.; Ramsay, D. A.; Lovas, F. J.; Lafferty, W. J.; Maki, A. G. *J. Phys. Chem. Ref. Data* **1979**, *8*, 619.
(35) (a) Murray, K. K.; Leopold, D. G.; Miller, T. M.; Lineberger, W. C. *J. Chem. Phys.* **1988**, *89*, 5442. (b) Koda, S. *Chem. Phys. Lett.* **1978**, *55*, 353. (c) Koda, S. *Chem. Phys.* **1982**, *66*, 383.
(36) Rao, D. R. *J. Mol. Spectrosc.* **1970**, *34*, 284.
(37) Demidov, A. V.; Gershikov, A. G.; Zasorin, E. Z.; Spiridonov, V. P.; Ivanov, A. A. *Zh. Struct. Khim.* **1983**, *24*, 7.
(38) Balasubramanian, K. *J. Chem. Phys.* **1988**, *89*, 5731.
(39) For recent high-level CI calculations on CF_2, see: Carter, E. A.; Goddard, W. A., III *J. Chem. Phys.* **1988**, *88*, 1752.
(40) Evangelisti, S.; Daudey, J. P.; Malrieu, J. P. *Chem. Phys.* **1983**, *75*, 91.
(41) (a) Schwerdtfeger, P.; Silberbach, H.; Miehlich, B. *J. Chem. Phys.* **1989**, *90*, 762. (b) Balasubramanian, K. *J. Chem. Phys.* **1989**, *91*, 2443.
(42) Zangrande, G.; Granozzi, G.; Casarin, M.; Daudey, J. P.; Minniti, D. *Inorg. Chem.* **1986**, *25*, 2872.

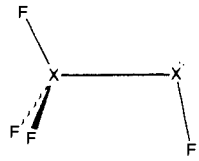

4

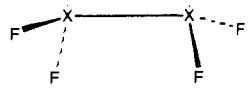

5

metry showed no critical points for any of the X_2F_4 surfaces. C_2F_4 relaxes, of couse, to the planar $F_2C{=}CF_2$ form while the other X_2F_4 isomers tend to dissociate into two singlet XF_2 units, as noted earlier by Krogh-Jespersen for Si_2F_4.[8]

The results are summarized in Table III for the geometries and in Table IV for the energies. Harmonic vibrational frequencies for the bridged forms are given in Table V. The calculated energies given in Table IV do not take into account the zero-point energy differences. These remain negligible within a series of X_2F_4 isomers while they disfavor X_2F_4 with respect to $2XF_2$ by ~ 2 kcal/mol (SCF level) whatever X. The energies discussed in the following are the CI-calculated relative energies. Let us now detail, for each kind of atom X, the shape of the X_2F_4 singlet surface.

C_2F_4. There are only two true minima: the stable planar ethylenic structure and the methylmethylene structure. The C_{2h} trans-bridged form is found to be a critical point of index 2, the two imaginary frequencies corresponding to the b_g mode **6** (730

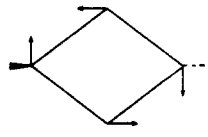

6

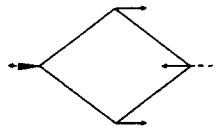

7

cm^{-1}) and the b_u mode **7** (313 cm^{-1}). The C_{2v} cis-bridged structure is also found to be a critical point of index 2, with two imaginary frequencies similar to the modes depicted in **6** and **7** [a_2 (729 cm^{-1}) and b_1 (302 cm^{-1}), respectively]. The two bridged forms are nearly degenerate in energy. They lie at 119 kcal/mol above the ethylenic isomer and are not bound with respect to two singlet CF_2. Note that **6** might lead to a dissociation into $2CF_2$ while **7** might lead to the methylmethylene form. This last structure $F_3C{-}CF$ is calculated to lie at 39 kcal/mol above the tetrafluoroethylene isomer and 17 kcal/mol below two singlet CF_2. Although F_3C substitution favors triplet states, $F_3C{-}CF$ is found to have a singlet ground state with a singlet–triplet separation of 9 kcal/mol.[43]

Si_2F_4. The planar form is found to be a saddle point with a single imaginary frequency corresponding to the trans bending mode (332 cm^{-1}). All the three other types of structures are found to be true minima. The absolute minimum, i.e., the structure lower in energy, is the silylsilylene form. The bridged forms are lying only a few kilocalories per mole in energy above this minimum. The C_{2h} trans-bridged form is preferred over the C_{2v} cis-bridged form by 0.5 kcal/mol. This preference, noticed also by Nagase and Kudo,[44] will be found in all our series (it also holds in the X_2H_4 series where, from silicon to lead, the trans-bridged structures are preferred by 2 kcal/mol over the cis-bridged ones).[26] All these three Si_2F_4 isomers are weakly bound with respect to two singlet SiF_2. The doubly bonded planar saddle point is high in energy and this trend will be reinforced for the heavier elements.

Ge_2F_4. Regarding the nature of the stationary points, this system deserves the same comments as those made on the preceding system. Relative energies are however quite different. The planar doubly bonded form is a saddle point with an imaginary frequency corresponding to trans bending (312 cm^{-1}). The bridged forms and the germylgermylene form are true minima. In Table V, the C_{2h} trans and C_{2v} cis-bridged forms of Ge_2F_4 both exhibit one imaginary frequency. Our SCF level of description actually gives a C_i-distorted trans-bridged form and a C_2-distorted cis-bridged form for Ge_2F_4. We will see later (see section V) that these distortions are, however, tiny and the barriers associated with their double wells are unsignificant. Therefore, these bridged forms can be virtually considered as C_{2h} and C_{2v}. The trans-bridged form is the most stable one and is bound by 24 kcal/mol with respect to two singlet GeF_2. The germylgermylene isomer $F_3Ge{-}GeF$ is lying at 32 kcal/mol above the bridged form and is unbound by 8 kcal/mol with respect to two GeF_2.

Sn_2F_4. Again, there are three true minima. The planar form is a saddle point with an imaginary frequency corresponding to trans bending (341 cm^{-1}). The trans-bridged isomer is the absolute minimum. The cis-bridged form is located less than 3 kcal/mol above in energy. The stannylstannylene form lies 60 kcal/mol higher in energy. The bridged forms are the only Sn_2F_4 isomers that are bound with respect to two singlet stannylenes SnF_2. Note also that the planar doubly bonded form is very high in energy.

Pb_2F_4. The bridged forms are the only true minima on the ground-state Pb_2F_4 potential surface. While the cis isomer is found to have a C_{2v} symmetry, the trans isomer is found to have a C_s-distorted symmetry. As in the case of germanium, however, the deformation is tiny and the energy associated with it is also tiny (see section V), so that trans-bridged Pb_2F_4 can be virtually considered as C_{2h}. The cis isomer lies 5 kcal/mol above the trans isomer. Both bridged forms are rather strongly bound with respect to two singlet PbF_2 fragments.

Optimizing a $F_3Pb{-}PbF$ structure keeping a C_s symmetry led to the geometry given in Table III, corresponding to an energy gradient of 0.0009. This geometry, however, has two low imaginary frequencies corresponding to in-plane tilting of the F_3Pb group and torsion about the PbPb bond. This structure, therefore is not a true minimum. Distorting it according to these modes and releasing any symmetry constraint did not permit any other critical point to be caught. The potential surface is very flat and further attempts to catch any other local minima failed. In particular, we attempted to find an unsymmetrical structure with a single fluorine bridge and a short Pb–Pb distance (such a geometry was found to be a local minimum for Pb_2H_4). The process did not converge on any stationary point corresponding to such a structure. We should emphasize that the optimization process around such nonsymmetrical conformations is extremely slow since the surface in these areas is very flat. Although we might have missed some nonclassical stationary point around the plumbylplumbylene form, we presume that there is actually no such local minimum. Note that the critical point resembling this isomer is high in energy (which may account for its nonminimum character).

The planar π-bonded form $F_2Pb{=}PbF_2$ is very high in energy and does not actually belong to the ground-state surface. It happens to be a true minimum on the first singlet excited-state surface. This surprising result deserves some attention. Remember that for building such a π-bonded planar adduct, one first has to promote each PbF_2 fragment into its open-shell $n_\sigma p_\pi$ $^3B_1$ state.[45] This requires so much energy ($2 \times 86 = 172$ kcal/mol; see Table I) that, even after building a $\sigma + \pi$ Pb=Pb bond, **8**, the system

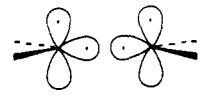

8

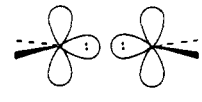

9

is still higher in energy than two singlet PbF_2 with the same geometry, **9**, having their n_σ lone pairs facing each other and undergoing a large repulsion.[46] **9** is located 34 kcal/mol below **8** (this is a vertical energy difference, referring to the optimized geometry of **8**). The upper limit of the energy required for bringing two repelling singlet PbF_2 to a distance as short as 2.50 Å is therefore 116 kcal/mol. This may seem a low value. In fact, it is a consequence of the inert-pair effect on PbF_2. The n_σ lone pair has a large s character and the 6s orbital of Pb is spacially contracted due to relativistic effects. The peculiar ordering is therefore a consequence of both the large singlet–triplet splitting

(43) Dixon, D. A. *J. Phys. Chem.* **1986**, *90*, 54.
(44) Nagase, S.; Kudo, T.; Ito, K. In *Applied Quantum Chemistry*; Smith, V. H., et al., Eds.; Reidel: Dordrecht, The Netherlands, 1986; p 249.
(45) Trinquier, G.; Malrieu, J. P. *J. Am. Chem. Soc.* **1987**, *109*, 5303.
(46) This corresponds stricto sensu to the diagram **9** of ref 25.

Table III. Calculated Geometries for the Stationary Points on the X_2F_4 Potential Energy Surfaces[a]

		C_2F_4	Si_2F_4	Ge_2F_4	Sn_2F_4	Pb_2F_4
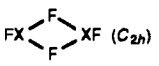 (C_{2h})	X···X	2.631	3.082	3.237	3.471	3.587
	X—F_b	1.697	1.906	1.998	2.113	2.201
	X—F_t	1.242	1.612	1.772	1.920	2.118
	F_bXF_b	78.4	72.2	71.6	69.6	70.9
	F_bXF_t	98.8	91.7	90.3	89.2	88.9
	XXF_t	101.4	92.1	90.3	89.0	88.6
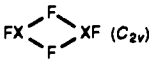 (C_{2v})	X···X	2.611	3.088	3.260	3.488	3.627
	X—F_b	1.695	1.908	2.005	2.119	2.208
	X—F_t	1.244	1.607	1.762	1.909	2.108
	F_bXF_b	78.5	71.9	71.2	69.1	69.3
	F_bXF_t	98.8	93.2	93.1	93.2	95.9
	XXF_t	107.5	92.5	92.1	90.9	94.2
	pucker.	12.2	2.8	3.4	2.3	5.9
F_3X—XF (C_s)	X—X	1.535	2.410	2.622	2.943	3.077
	X—F_1	1.279	1.621	1.772	1.914	2.092
	X—F_2	1.314	1.599	1.752	1.898	2.104
	X—F_3	1.323	1.597	1.747	1.894	2.083
	XXF_1	103.4	94.0	90.3	88.4	90.3
	XXF_2	110.8	110.6	113.7	115.2	104.2
	XXF_3	110.5	113.5	114.6	115.2	120.6
	F_3XF_3	108.6	106.9	105.5	104.8	104.1
$F_2X{=}XF_2$ (D_{2h})	X=X	1.302	2.048	2.174	2.470	2.499
	X—F	1.302	1.591	1.733	1.880	1.944
	FXF	112.7	109.7	108.0	107.2	106.5
$F_2\dot{X}$—$\dot{X}F_2$ ^3B (C_2)	X—X	1.494	2.330	2.508	2.826	2.943
	X—F_0	1.310	1.606	1.757	1.901	2.103
	X—F_i	1.317	1.604	1.751	1.895	2.105
	XXF_0	113.7	106.3	105.3	104.0	96.0
	XXF_i	115.8	115.0	113.8	114.1	115.4
	F_iXF_0	110.3	106.9	105.8	104.5	108.4
	F_iXXF_i	64.1	55.3	49.8	45.6	42.2
	F_iXXF_0	65.2	62.8	65.6	67.6	71.5

[a] In angstroms and degrees. See Figure 1 for labeling.

Table IV. Calculated Relative Energies (kcal/mol)

	SCF					CI				
	C	Si	Ge	Sn	Pb	C	Si	Ge	Sn	Pb
$2XF_2$ ($^1A_1$)	49.0	10.8	28.4	57.0	68.7	56.3	6.3	23.8	50.9	62.3
$F_2\dot{X}$—$\dot{X}F_2$ (^3B)	26.0	26.8	66.8	100.4	156.9	44.0	38.8	74.6	102.4	134.4
$F_2X{=}XF_2$	0	57.9[a]	110.3[a]	155.3[a]	240.0	0	50.5	97.3	133.1	212.2
F_3X—XF	28.5	0	34.0	64.9	100.4[a]	38.9	0	32.1	60.0	88.7
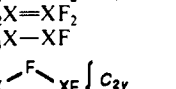 C_{2v}	123.6[a]	9.5	2.9	4.3	6.5	118.9	4.2	1.9	2.6	4.8
C_{2h}	123.8[a]	8.5	0	0	0	118.8	3.7	0	0	0

[a] Not true minimum.

in PbF_2 and the relativistic spacial contraction of the n_σ lone pair in singlet PbF_2. The CI expansions for these two states show contributions of 80% of **9** and 13% of **8** for the ground singlet state and 80% of **8** and 12% of **9** for the first excited singlet state. Usually, the π-bonded structure **8** is the *lower* state and the mixing of **8** and **9** produces a *weakening* of the trans-wagging force constant, possibly making it negative. In the present case where the π-bonded structure **8** is the *upper* state, we may expect, as a consequence of the mixing, a *strengthening* of the trans-wagging force constant, as in classical interaction diagrams. This is what happens. The trans-wagging frequency in planar π-bonded $F_2Pb{=}PbF_2$ is pushed up to 922 cm^{-1}, which is far above the other frequencies.

Now that we have detailed the singlet surfaces, what about the diradical triplet species $F_2\dot{X}$–$\dot{X}F_2$? These species have been optimized in a C_2 symmetry. All of them happen to be true minima. Their geometrical parameters are given in Table III. These states are not favored with respect to the planar π-bonded form for $F_2C{=}CF_2$ or with respect to the bridged forms for the heavier analogues. For C_2F_4, the ^3B triplet state is located at 44 kcal/mol above the tetrafluoroethylene ground state. This is only 5 kcal/mol above singlet tetrafluoromethylmethylene. For Si_2F_4, the triplet state is located at 12 kcal/mol below the singlet planar saddle point (at the SCF level, this difference is 31.1 kcal/mol, in excellent agreement with ref 8). This is still 35 kcal/mol above the bridged form. For the heavier molecules, the twisted triplet state is located lower and lower below the planar saddle point but higher and higher above the bridged form and the methylmethylene-type form (see Table IV).

B. General Shapes. Turning back to the singlet surface, let us now try to summarize its features, focusing first on the competition between the F_3X–XF isomer and the bridged isomer (as from now, we shall consider only its trans form in the discussion). The hypothetical and arbitrary C_s pathway **10**, which connects

10

two degenerate forms of staggered F_3X–XF through the trans-bridged form, will help us to understand the trends along the series. The corresponding energy profiles are schematized in Figure 2. The relative stability of the bridged form regularly increases from Si to Pb. For Si_2F_4, the F_3Si–SiF form is still preferred. From Ge_2F_4 to Pb_2F_4, the bridged form is the preferred one, with increasing stability. In the two extreme cases, one of the two isomers is high in energy and is no longer a true minimum. This is F_3Pb–PbF on the Pb_2F_4 surface and the bridged form on the C_2F_4

Table V. Harmonic Vibrational Frequencies (cm^{-1}) and Their Assignments, for the Bridged Structures[a]

Si_2F_4						Ge_2F_4									
C_{2h}			C_{2v}			C_{2h}		C_i			C_{2v}		C_2		
b_u	84	r + p	a_1	95	s + p	b_g	52i	a_g	91	ν_b	a_2	81i	a	101	ν_b
b_g	98	ν_b	a_2	111	ν_b	b_u	60	a_u	60	r + p	a_1	82	a	82	s + p
a_u	181	w	a_2	181	t	a_u	141	a_u	140	w	a_2	124	a	125	t
a_g	218	s	b_1	263	r	a_g	154	a_g	156	s	b_1	180	b	176	r
b_g	295	t	b_2	274	w	b_g	244	a_g	245	t	a_1	214	a	223	b + p
b_u	394	p + r	a_1	314	p + b + s	a_g	279	a_g	283	b + s	b_2	220	b	224	w
a_u	432	ν_b	b_2	436	ν_b	a_u	306	a_u	297	ν_b	b_2	304	b	301	ν_b
a_g	461	b	b_1	465	ν_b	b_u	316	a_u	316	p + r	b_1	321	b	371	ν_b
b_u	464	ν_b	a_1	492	b + p + s	b_u	328	a_u	367	ν_b	a_1	332	a	333	p + s
a_g	559	ν_b	a_1	563	ν_b	a_g	440	a_g	447	ν_b	a_1	441	a	452	ν_b
a_g	1006	ν_1	b_1	1007	ν_1	a_g	717	a_g	717	ν_1	b_1	724	b	724	ν_1
b_u	1021	ν_1	a_1	1028	ν_1	b_u	726	a_u	726	ν_1	a_1	737	a	737	ν_1

Sn_2F_4						Pb_2F_4							
C_{2h}			C_{2v}			C_{2h}		C_s			C_{2v}		
b_u	49	r + p	a_1	76	s + p	b_u	23i	a'	20	r + p	a_1	65	s + p
a_u	118	w	a_2	93	t	a_g	85	a'	94	s	a_2	67	t
a_g	124	s + b	b_1	136	r	a_u	98	a''	99	w	b_1	93	r
b_g	208	t	a_1	191	b + p	a_g	166	a'	168	b + s	a_1	151	b + p
a_g	228	b + s	b_2	194	w	b_g	181	a''	184	t	b_2	158	w
b_u	274	p + r	a_1	280	p + s	b_u	228	a'	233	p + r	a_1	218	p + s
a_u	372	ν_b	b_2	370	ν_b	a_u	521	a'	527	ν_b	b_2	502	ν_b
b_g	403	ν_b	a_2	402	ν_b	a_g	583	a'	586	ν_b	a_1	574	ν_b
a_g	483	ν_b	a_1	485	ν_b	b_u	632	a'	637	ν_1	b_1	603	ν_1
b_u	493	ν_b	b_1	495	ν_b	a_g	634	a'	626	ν_1	a_1	615	ν_1
a_g	640	ν_1	b_1	673	ν_1	b_g	658	a''	654	ν_b	a_2	645	ν_b
b_u	647	ν_1	a_1	681	ν_1	b_u	721	a'	718	ν_b	b_1	708	ν_b

[a] The assignments are labeled as follows: ν_1, XF_1 stretching; ν_b, XF_b stretching; b, XF_b in-plane bending; p, ring puckring; s, XF_1 scissoring; r, XF_1 rocking; w, XF_1 wagging; t, XF_1 twisting.

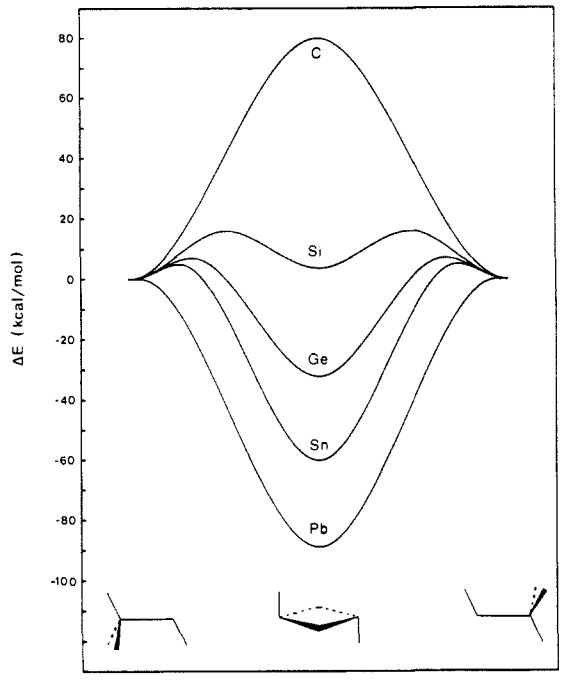

Figure 2. Schematic energy profiles linking the methylmethylene forms and the bridged forms.

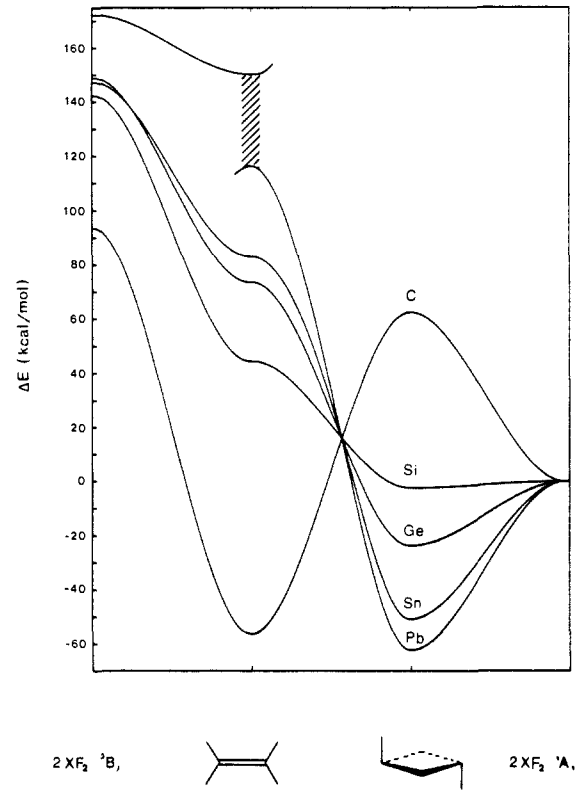

Figure 3. Schematic energy profiles linking, from right to left, $2XF_2$ ($^1A_1$), the C_{2h} trans-bridged form, the D_{2h} planar π-bonded form, and $2XF_2$ ($^3B_1$). The reaction coordinate is arbitrary.

surface. Figure 2 shows some regularity along the series.

A second point concerns the relative positions of the bridged and planar forms with respect to the two isolated XF_2 fragments, both in their $^1A_1$ and $^3B_1$ state. To illustrate this aspect of the singlet potential surface, let us consider the arbitrary reaction coordinate **11**. Starting from the right-hand-side asymptote, two

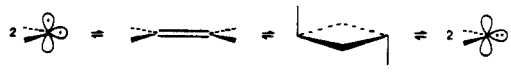

11

singlet ground-state XF_2 fragments are coupled to build the bridged form. Then, moving to the left, the bridged form is converted into the planar π-bonded form (through a pathway that we will assume to be monotonous, due to the significant energy

differences between these two forms). Lastly, on the left-hand-side asymptote, the planar ethylenic form is dissociated into its "natural" building blocks, which are the two coupled triplet XF_2 fragments. The energy profiles for this section of the X_2F_4 surfaces are given in Figure 3 in which zero energy corresponds to the separate singlet fragments. The binding energy of the bridged form with respect to $2XF_2$ ($^1A_1$) regularly increases from silicon to lead (in the range 3–62 kcal/mol; see Table IV). This is in sharp contrast with the X_2H_4 bridged compounds, which were found to be equally bound with respect to $2XH_2(^1A_1)$, including the case of C_2H_4.[26] Note that here C_2F_4 is largely unbound with respect to $2CF_2(^1A_1)$. This is a first illustration of the fundamental difference between the fluorine bridges (three-center four-electron bonds) and the hydrogen bridges (three-center two-electron bonds).

Moving from the bridged structure to the planar π-bonded structure produces various shapes according to the nature of the X atom. For silicon, germanium, and tin, one rises in energy from the bridged minimum to the π-bonded planar saddle point, which is a plateau point in Figure 3. Note that the deeper the bridged minimum, the higher the planar saddle point. For carbon, the energy curve drops from the bridged critical point (a maximum in Figure 3) to the deep well of the ethylenic minimum. For lead, one cannot reach the π-bonded structure since it belongs to the second singlet surface. The vertical separation between the two surfaces is shown by the shaded strip in Figure 3. On the ground-state surface, the planar geometry corresponds to the nonstationary point **9** (a maximum on the Pb curve of Figure 3).

Dissociating the ethylenic planar form into $2XF_3(^3B_1)$ results in the loss of the $\sigma + \pi$ bond energy. This also applies to the excited singlet surface of Pb_2F_4, but there, due to the interaction with the ground-state surface, the π-bonded form is pushed up in energy, reducing therefore the $\sigma + \pi$ increment. The left part of Figure 3 shows that this intrinsic $\sigma + \pi$ bond energy is large for carbon and, as expected, reduced for the heavier elements. The following $\sigma + \pi$ increments are obtained (in kcal/mol): C, 150; Si, 98; Ge, 75; Sn, 65.

Note that for C_2F_4, this number is smaller than that obtained for C_2H_4, while for Si_2F_4, it is larger than that obtained for Si_2H_4. For germanium and tin, these $\sigma + \pi$ increments are similar to those obtained in the X_2H_4 series.[26]

Figure 3 makes the singularity of the C_2H_4 surface conspicuous with respect to its heavier analogues. By far $F_2C{=}CF_2$ is the only doubly bonded molecule in the series that is a true minimum and is bound with respect to its constituent singlet fragments. None of the other heavier $F_2X{=}XF_2$ analogues are any longer minima. Moreover, they are very high in energy, not only above the bridged structures, but also above the $F_3X{-}XF$ isomers (not shown in Figure 3). The singularity of lead in these curves comes from the large ΔE_{ST} and the contracted character of the n_σ pair in PbF_2, as well as from the weak $\sigma + \pi$ Pb=Pb bond energy. However, this singularity occurs at a higher zone of energy and has practically no structural consequence for the preferred bridged isomer. The carbon singularity, on the other hand, is quite dramatic since it gives a shape of the potential energy surface that is nearly the reversed symmetrical part of that of the heavier elements. In particular, the binding energy of $F_2C{=}CF_2$ with respect to two singlet ground-state CF_2 (right-hand-side asymptote) is comparable to that of bridged Pb_2F_4 with respect to $2PbF_2$. From the planar maxima in Figure 3, it is also possible, of course, to fall back to the $2XF_2$ ($^1A_1$) asymptote by trans bending and XX stretching. When this asymptote is common to both sides, one obtains the curves plotted in Figure 4. The difference between first-row and following-row atoms is even more clearly illustrated in this figure. Comparing these surface shapes with those obtained for X_2H_4 by similar methods (Figure 4 of ref 26) illustrates how the bonding in the doubly bridged hydrogen compounds must be different from that in the fluorine analogues. On the X_2H_4 surface, the peculiarity of carbon over its heavier elements was also shown for the stability of the π-bonded forms. One of the reasons behind this is, of course, the privileged status of the $2p_z$–$2p_z$ overlap.

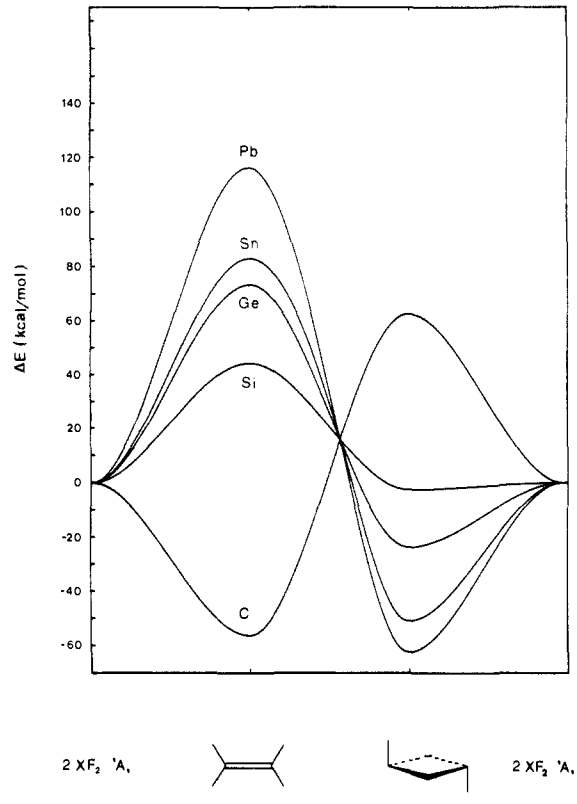

Figure 4. Schematic energy profiles linking the C_{2h} trans-bridged form, the D_{2h} planar π-bonded form, and the common asympote $2XF_2$ ($^1A_1$).

V. Comments on the Structures

A. Bridged Forms. 1. Distortions. In its C_{2h} geometry, trans-bridged Ge_2F_4 exhibits an imaginary frequency corresponding to the b_{2g} symmetry-breaking of the ring, **12**. When

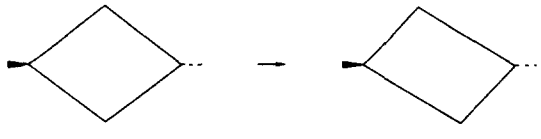

12

reoptimized with reduced C_i symmetry, the bridge Ge–F_b bonds are of two types with rather small differences (Ge–F_b = 2.037 and 1.963 Å; F_bGeF_b = 71.7°; F_tGeF_b = 89.9° and 90.7°). The energy benefit due to this symmetry breaking is negligible at the SCF level (1 cm^{-1}). Exploring the distortion at the MP2 level also led to a very flat curve with an energy lowering of only 4 cm^{-1} (0.01 kcal/mol). In the C_i-optimized geometry, trans-bridged Ge_2F_4 now exhibits only real frequencies (see Table V). The a_g mode corresponding to the restitution of a C_{2h} symmetry has a frequency of 91 cm^{-1}. This corresponds to a zero-point energy of 0.1 kcal/mol, which is much higher than the barrier separating the two C_i minima. Therefore, although a double-well problem may exist for such bridged structures, the barrier separating the two C_i-distorted forms is below the first vibrational energy level, so that the distortion should not be detectable. It may be asked whether the appearance and extent of such a distortion is sensitive or not to the inclusion of polarization d orbitals on the bridging fluorine atoms. The C_{2h} and C_i forms of Ge_2F_4 were reexplored with a basis set including the polarization orbitals on the bridging atoms. The distortion is maintained and slightly enhanced. The SCF energy difference between the two forms is now 9 cm^{-1} and the geometry of the C_i form corresponds to the following parameters: Ge–F_b = 2.050 and 1.902 Å; F_bGeF_b = 73.3°; F_tGeF_b = 89.2° and 91.0°.

In the solid state, the bridged Ge_2F_4 units actually exhibit such a distortion.[14] Although the double-well barrier is very weak for isolated molecules, intermolecular and collective effects may

Table VI. Some Differences between the Hydrogen-Bridged[a] and Fluorine-Bridged Parent Molecules

	X_2H_4	X_2F_4
particularity of the carbon isomer	structurally singular; bound with respect to $2CH_2$ ($^1A_1$)	structurally homogeneous; unbound with respect to $2CF_2$ ($^1A_1$)
binding energy with respect to $2XR_2$ ($^1A_1$)	rather constant around 30 kcal/mol	variable from 3 to 62 kcal/mol
valence angle on the bridging atom	$\hat{H}_b$ = 103–106°	$\hat{F}_b$ = 108–110°
relative X–R bond lengthening from XR_2 ($^1A_1$) to X–R_b	rather constant around 10%	variable from 32% to 4%
ring distortion	not found	found for Ge_2F_4 and Pb_2F_4

[a] Reference 26.

enhance it and trap one of the two distorted forms in the molecular crystal. This experimental geometry corresponds to Ge–F_b = 2.09 and 1.91 Å and F_bGeF_b = 85°, which we consider to agree satisfactorily with the above-mentioned SCF geometry. In Table V, note that the distortion practically does not alter the calculated vibrational frequencies for trans-bridged Ge_2F_4. There is a one-to-one correspondence between the g and u modes for the two sets. Vibrational spectroscopy cannot therefore discriminate between the two forms since both maintain an inversion center. The assignments made from our calculated force fields may help to ascertain those made in ref 19. As can be seen in Table V, no ν_{GeGe} frequency was assigned to any mode since there is no direct GeGe link in the molecule, as there is no direct XX link in any of the other bridged structures considered in this work. The mode that would correspond to GeGe stretching is the symmetrical in-plane bending deformation of the ring (denoted b in Table V) at 279 cm^{-1}. This is fortuitously close to ν_{GeGe} calculated in $F_2\dot{G}e$–$\dot{G}eF_2$ (^3B).

Similarly, cis-bridged Ge_2F_4 undergoes a $C_{2v} \rightarrow C_2$ distortion, **13**, associated with a very weak energy gain (6 cm^{-1} at the SCF

13

level). The C_2-optimized geometry exhibits tiny differences with respect to the C_{2v} geometry (Ge–F = 2.058 and 1.959 Å; F_bGeF_b = 71.2°; F_tGeF_b = 92.7 and 93.4°). Again, the "a" frequency associated with the recovery of C_{2v} symmetry, 101 cm^{-1}, corresponds to a zero-point energy that is largely above the double-well barrier.

Trans-bridged C_{2h} Pb_2F_4 exhibits a weak imaginary frequency corresponding to distortion **14**. Reoptimizing this trans-bridged

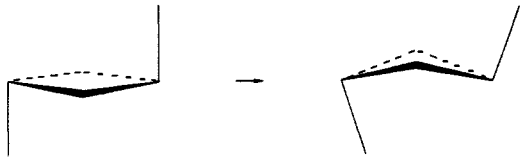

14

form under a lowered C_s symmetry constraint led to tiny changes in the geometry (Pb–F_b = 2.198 and 2.205 Å; Pb–F_t = 2.121 and 2.119 Å; F_bPbF_b = 71.1° and 70.8°; puckering = 12.8°; F_tPbF_b = 85.5° and 90.9°; $PbPbF_t$ = 78.1° and 97.3°) associated with an energy gain of only 40 cm^{-1}. Therefore, in this case the distortion could be seen. Note in Table V that the frequencies for the C_s form are all real and are quite close to those of the C_{2h} form. In contrast with Ge_2H_4, the b_g mode corresponding to the ring deformation **12** is now associated with a rather high frequency (654 cm^{-1}).

2. Geometries. All the doubly bridged structures are rhombuses with an acute angle at X of 78° for carbon and 72–70° for silicon to lead. This makes a valence angle on the fluorine bridge of 108–110° for Si to Pb. As can be seen in Table III, the geometrical parameters are rather similar in the trans and cis isomers. The C_{2v} symmetry of the cis isomer allows a puckering of the ring, but this remains very weak. As observed on the X_2H_4 bridged

Table VII. Net Atomic Charges on Singlet XF_2 and Trans-bridged X_2F_4

	XF_2 ($^1A_1$)		X_2F_4 (^1A_g)		
	X	F	X	F_b	F_t
C	+0.34	−0.17	+0.60	−0.52	−0.08
Si	+0.95	−0.47	+1.11	−0.63	−0.49
Ge	+1.12	−0.56	+1.18	−0.62	−0.57
Sn	+1.32	−0.66	+1.34	−0.68	−0.66
Pb	+1.34	−0.67	+1.36	−0.69	−0.68

compounds, the weak folding of the ring occurs on the side of the terminal C–F_t bonds as in **15**. In C_2F_4, however, the folding

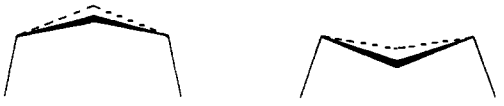

15 16

occurs on the other side, **16**. The planar four-membered rings of all the C_{2h} trans-bridged isomers have a similar shape, including the C_2H_4 isomer, which is not a true minimum. The extracyclic X–F_t bonds are close to those in singlet XF_2. The bridge X–F_b bonds are of course longer, but their relative lengthening with respect to XF_2 ($^1A_1$) decreases along the series (C, +32%; Si, +18%; Ge, +13%; Sn, +10%; Pb, +4%). Because these X–F_b bond lengths run from 1.70 (C) to 2.20 Å (Pb), the cross-ring X···X distances are rather long. There is, hence, no question of direct intraring X···X interaction, as could be debated in the X_2H_4 bridged geometries. The angles between the four-membered rings and the extracyclic X–F_t bonds run from 92° (Si) to 89° (Pb), with a more open value in the case of carbon (101°). Because of the puckering, the XXF_t values of Table III are slightly larger in the cis isomers. All F_tXF_b angles are slightly shorter than in XF_2 ($^1A_1$). For the trans isomers, when going down to the heavier elements, the decrease of both F_tXF_b and XXF_t angles make the structures somewhat more compact.

At this point we can draw up the energetic and structural differences between the hydrogen bridges encounted in X_2H_4 and the fluorine bridges encountered in X_2F_4. This is done in Table VI. Energetically, the hydrogen-bridged structures are equally bound (by ≃30 kcal/mol) with respect to $2XH_2$ ($^1A_1$), while the fluorine-bridged structures have binding energies, regarding $2XF_2$ ($^1A_1$), that depend on X (in particular, when X = C, the bridged structure is unbound). Structurally, the rings have about the same shape, with an obtuse angle at the bridging atom. This may be understood by simple electrostatic arguments. The rings bear alternating X^+–F^- charges with the positive charge on X being larger than the negative one on F, thus inducing larger repulsion. The calculated net charges on the XFXF rings, given in Table VII, are larger than those on the XHXH rings, so that the XFXF rhombuses may be expected to be more prolate than the XHXH ones. This is what is actually observed. As mentioned, the main structural difference between these two kinds of rings is that the X–F_b bond lengths no longer permit a short X···X contact in X_2F_4.

3. Electronic Structures. In the X_2H_4 bridged structures, the bonding was analogous to that in diborane, namely, two three-center two-electron bonds (also called electron-deficient bonds) each bridge involving two electrons and three orbitals localizable as in **17**. In X_2F_4, the two bridge bonds involve four electrons and four orbitals localizable as in **18**, since the fluorine brings an

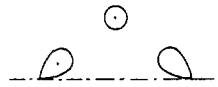

17

18

in-plane lone pair besides its unpaired electron. The strong charge alternation observed on such rings (see Table VII) suggests that these structures are significantly stabilized by electrostatic effects. A naive electrostatic picture suggests that a direct X=X coupling of two highly polarized F^-—X^+—F^- species is an unfavorable process, while the right pairing of two X^+—F^- dipoles should produce a more favorable four-membered ring. So, when the X–F bonds are strongly polar, the system prefers to displace the unsaturation to a ring bearing alternating X^+–F^- charges. One could be tempted to consider the adduct as being bound by two dative bonds from a fluorine lone pair into the p_π empty orbital of its partner, the two carbenic n_σ lone pairs keeping out of the bonding, **19**. In such a case, the X–F bonds should reduce their polarity

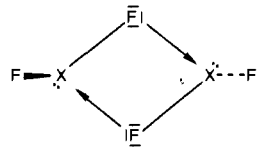

19

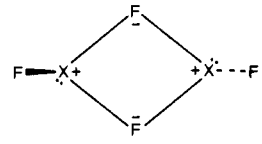

20

when going from isolated fragments to the ring form. This is not supported by the increase in the X^+–F_b^- polarity when compared to that in isolated XF_2. The following increases in the F_b negative charge are obtained: C, −0.35; Si, −0.16; Ge, −0.06; Sn, −0.02; Pb, −0.02.

The bonding in the four-membered ring is therefore mainly ionic and best depicted by **20**. In a valence-bond (VB) wavefunction we would therefore expect a significant weight for the determinant associated to configuration **20**. For the X_2H_4 series, where the electronegativities of X and H are less contrasted, such a VB form was found to have a weight of only 2–3% according to our orthogonal VB analyses.[47]

B. Other Forms. $F_2X{=}XF_2$. For C_2F_4, the present work compares favorably with literature calculated values,[1,5] while giving too short bond lengths when compared to experiment (CC = 1.311 Å; CF = 1.319 Å; FCF = 112.3°).[48] The XX bond shortening occurring from F_3X—XF to $F_2X{=}XF_2$ is rather large and fairly constant within the series (15–19%). The X=X bond shortening resulting from the perfluorosubstitution in $H_2X{=}XH_2$ is also constant around 3% from Si to Ge.

F_3X–XF. For X = C and Si, our geometries are in good agreement with those calculated at the SCF level by Dixon[43] on F_3C–CF and Krogh-Jespersen[8] on F_3Si–SiF. The $-XF_1$ part of F_3X–XF is quite similar to that in singlet XF_2. The X–X–F_1 angles are ~90°, and decrease with heavier elements. Note that for F_3Sn–SnF, the valence angle on the stannylene part is now an acute angle (88°). In Table III, do not pay too much attention to the parameters for F_3Pb–PbF since this is not a true minimum, as mentioned above. When comparing these X–X bond lengths with those calculated in the H_3X–XH series, it may be pointed out that the fluorine substitution increases the X—X bond lengths, unlike the case of $H_2X{=}XH_2$.

$F_2\dot{X}$–$\dot{X}F_2$. The X–X single bond lengths in these species are shorter than those in F_3X–XF. On the other hand, they are longer than those in ethane-like F_3X–XF_3, where fluorine substitution is known to shorten the X–X bonds. With the same basis sets, the Sn–Sn and Pb–Pb bond lengths in D_{3d} Sn_2F_6 and Pb_2F_6 were optimized at 2.775 and 2.809 Å, respectively. As expected, each X atom in $F_2\dot{X}$–$\dot{X}F_2$ is strongly pyramidalized. This may be accounted for directly from the pyramidal geometry of the $\dot{X}F_3$ radicals. Note in particular the pyramidal carbons in ^3B C_2F_4,

(47) Trinquier, G.; Malrieu, J. P.; Garcia-Cuesta, I., manuscript in preparation.

(48) Carlos, J. L.; Karl, R. R.; Bauer, S. H. *J. Chem. Soc., Faraday Trans. 2* **1974**, *70*, 177.

Table VIII. Calculated Vertical First Ionization Energies (eV)[a]

		C	Si	Ge	Sn	Pb
XF_2	n_σ	13.03	11.32	11.94	11.42	12.30
					(11.66)	(12.06)
F_3X—XF	n_σ	12.47	10.15	10.91	10.57	11.36
X_2F_4						
C_{2h}	n^-	12.66	10.77	11.31	10.80	11.85
					(10.88)	(11.77)
	n^+	14.76	12.01	12.44	11.73	12.60
					(11.82)	(12.33)
C_{2v}	n^-	13.00	10.83	11.31	10.76	11.71
	n^+	14.20	12.07	12.28	11.61	12.39
$F_2X{=}XF_2$	π_{xx}	11.32	8.50	8.82	8.35	8.18

[a] Highest energy levels from the SCF calculations. The numbers in parentheses are the values corrected from repolarization and correlation effects according to the procedure of ref 42.

whereas these are planar in the parent triplet $^3A_2$ (D_{2h}) C_2H_4.[49] Our results are in excellent agreement with those of Wang and Borden[5] for C_2F_4 and those of Krogh-Jespersen[8] for Si_2F_4. As reflected by the dihedral angles in Table III, the twisting of the two pyramidal F_2X groups is rather constant within the series. It makes possible both a nearly coplanar F_0XXF_0 arrangement, **21**, and the expected orthogonal orientation of the orbitals containing the unpaired electrons.

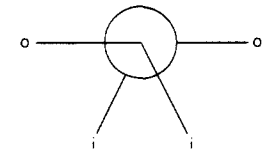

21

VI. Comparison with Spectroscopic Data for Sn_2F_4 and Pb_2F_4

Our results indicate a rather strong binding energy for the bridged structures of Sn_2F_4 and Pb_2F_4. As previously mentioned, there is strong evidence for formation of Sn_2F_4 both in condensed phase and in the gas phase. For the gas-phase dimerization of SnF_2, mass spectrometric studies give an enthalpy of $\Delta H_{298}° = -39 \pm 2$ kcal/mol,[20] which is in line with our calculated $\Delta H_0° = -49.6$ kcal/mol. The vibrational frequencies calculated for C_{2h} Sn_2F_4 may be compared with the infrared-active bands observed on matrix-isolated Sn_2F_4.[21] When corrected by a scaling factor of 0.9, the agreement is reasonable and we confirm the assignments made in ref 21:

	SCF (cm^{-1})	exptl (Ne, Ar) (cm^{-1})
b_u	582	580–590
b_u	444	384–393
a_u	335	333–339
b_u	247	220–233

The first ionization energies for all XF_2 monomers and X_2F_4 bridged dimers are given in Table VIII. For Sn_2F_4, an ionization energy of 10.63 eV has been proposed, from the photoelectron spectrum of gas-phase SnF_2, assumed to include some proportion of dimer.[24] The calculation of ionization energies for SnF_2 and Sn_2F_4 was performed both by using Koopmans' theorem (KT) and including corrections for repolarization and correlation effects.[42] The results are summarized in Figure 5. All the assignments made in ref 24 are confirmed. Note in particular that the second ionization energy n^+ of the dimer, corresponding to the bonding combination of the n_σ lone pairs, should be concealed in the band at 11.5 eV. Similarly, four levels corresponding to fluorine lone pairs in the dimer are calculated around 13.8 eV (after corrections, and not shown in Figure 5). These should be concealed in the clump centered at 14.0 eV.

In sharp contrast with SnF_2, the mass spectrometric studies do not support formation of any dimer in gas-phase PbF_2. This has been rationalized by the competition of dimerization with the

(49) Kohler, H. J.; Lischka, H. *J. Am. Chem. Soc.* **1982**, *104*, 5884.

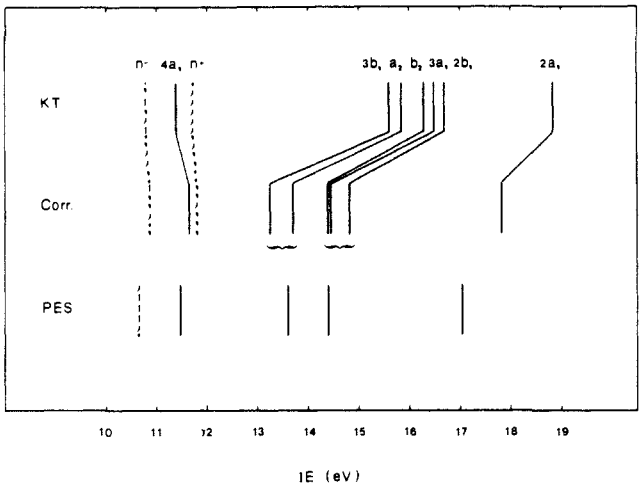

Figure 5. Calculated and observed vertical ionization energies for SnF_2 monomer (full lines) and dimer (broken lines). KT stands for Koopmans' theorem level. Corr means after repolarization and correlation corrections. PES data from ref 24.

Table IX. Some SCF-Estimated Reaction Energies[a]

	$2XF_2 \rightarrow XF_4 + X$	$XF_4 + X \rightarrow X_2F_4$	$XF_2 + F_2 \rightarrow XF_4$
C	+4.0	−53.5	−189.6
Si	+1.6	−12.9	−242.5
Ge	+37.6	−66.0	−167.7
Sn	+51.5	−108.0	−154.1
Pb	+105.8	−173.8	−70.9

[a] In kilocalories per mole. Each species is in its ground state: X, ^3P; XF_2, $^1A_1$; C_2F_4, π-bonded form; Si_2F_4, F_3Si–SiF; other X_2F_4, trans-bridged form.

disproportionation process $2PbF_2(g) \rightarrow PbF_4(g) + Pb(g)$, which would be thermodynamically more favorable, the enthalpy being estimated at −5 to −20 kcal/mol.[20] In Table IX, we report the energy concerning these reactions, calculated at the SCF level. For SiF_2, the SCF-calculated disproportionation energy is quite reasonable when compared with the corresponding experimental enthalpy $\Delta H_{298}° = +2.9$ kcal/mol.[50] The disproportionation of PbF_2 into PbF_4 + Pb appears as a very unfavorable process. The process is more and more difficult when going down column 14. This is not surprising from the known relative preference for divalence in heavier group 14 elements, and in particular with lead. Therefore, according to our results, no thermodynamic factor would prevent the formation of a dimer Pb_2F_4 in the gas phase. To end with these thermodynamic comments, it must be pointed out that the peculiarity of lead regarding the calculated energies of Table IX comes from the rather weak atomization energy found for PbF_4 at our SCF level (147 kcal/mol), which is not in agreement with the literature value (270 kcal/mol).[51]

In the PES spectrum of gas-phase PbF_2, no band was assigned to the dimer.[24] According to our calculations, the highest energy level in PbF_2 ($4a_1$,n_σ) is located at 12.1 eV while the first ionization energy of the dimer Pb_2F_4 (n^-) is located at 11.8 eV. The existence of the dimer would not therefore be in contradiction with the observed first ionization energy, at 11.8 eV. However, our calculations would locate additionally a set of six levels corresponding to fluorine lone pairs of PbF_2 (two levels) and Pb_2F_4 (four levels) within the interval 12.0–12.1 eV—a feature that has nothing to do with the experimental PES spectrum. Maybe our calculated ionization energies are not reliable for PbF_2 since we neglect some effects, such as spin–orbit coupling. Infrared-active frequencies have been reported for a presumed bridged Pb_2F_4 dimer.[21] Our calculated frequencies, however, do not confirm these values or their assignments. In conclusion, our results confirm the spectroscopic data of Sn_2F_4, whereas they do not seem to support any assignments for spectroscopic data of Pb_2F_4. The nonexistence of Pb_2F_4 would, however, be in contradiction with its rather enhanced stability with respect to $2PbF_2$.

VII. Summary and Conclusion

In this work, we established the existence of stable doubly bridged forms for the heavier analogues of tetrafluoroethylene. For Si_2F_4, the bridged form is nearly degenerate in energy with the silylsilylene isomer, and it is hardly favored with respect to its dissociation product. This is not in contradiction with the existence of SiF_2 as a covalent polymer rather than a molecular crystal involving dimers or low oligomer units. With germanium, tin, and lead, the bridged forms are definitely the preferred ones, with rather large binding energies regarding $2XF_2$. This accounts for the observed formation of bridged dimers in solid-state GeF_2, but it does not explain why, in the same conditions, SnF_2 forms bridged tetramers whereas PbF_2 is a pure ionic crystal. Once more,[52] carbon behaves as an exception in the series since its bridged forms are not real minima and are largely unbound. The four-membered rings may undergo small distortions from their higher symmetry, as shown for Ge_2F_4 and Pb_2F_4. The resulting double wells are, however, so flat that the deformation should hardly be detectable on isolated molecules. Only collective effects may evidence such a distortion in the solid state, as observed with Ge_2F_4.

The present results, which required a large amount of computing time, bring new structural and energetic data. They also raise some questions. Would higher levels of description change the shapes of the potential energy surfaces? Why is the surface so flat around the four-membered rings? Would inclusion of spin–orbit coupling significantly change our geometries and our calculated relative energies for tin and lead compounds? A complete optimization of a bridged structure at the CI level seems desirable to settle the influence of correlation effects on these cyclic geometries. The conspicuous differences between the hydrogen bridges and the fluorine bridges would need to be rationalized. In particular, a detailed study of the electronic structure of these three-center four-electron bridges should be made, grounding both on one-electron arguments and valence-bond analyses, as was performed on hydrogen-bridged[47] and lithium-bridged systems.[53] Maybe the most puzzling question concerns the structure of the carbon-containing heterofluoroolefins such as $CSiF_4$. Are such molecules bridged or doubly bonded? Work is in progress along these lines.

Acknowledgment. We are grateful to the C.N.R.S. for a generous grant of CPU time on the VP200 computer of the C.I.R.C.E.

Supplementary Material Available: Tables of basis sets and pseudopotential parameters (7 pages). Ordering information is given on any current masthead page.

(50) Farber, M.; Strivastava, R. D. *J. Chem. Soc., Faraday Trans.* **1978**, *74*, 1089.
(51) *JANAF Thermochemical Tables*, 3rd ed. *J. Phys. Chem. Ref. Data* **1985**, *14* (Suppl. 1).
(52) Kutzelnigg, W. *Angew. Chem., Int. Ed. Engl.* **1984**, *23*, 272.
(53) Epiotis, N. D. *Lect. Notes Chem.* **1982**, *29*, 1; *Ibid.* **1983**, *34*, 1; *Nouv. J. Chim.* **1988**, *11*, 231, 257, 303.